Supporting Information

for

Internal Water and Microsecond Dynamics in Myoglobin

Shuji Kaieda and Bertil Halle

Department of Biophysical Chemistry, Lund University, PO Box 124, SE-22100 Lund, Sweden

Table S1. Samples for MRD Experiments.

#	C_{Mb}[a]	type[b]	N_{GA}	pD	buffer[c]	nuclide	range (MHz)	n[d]
1	1.98	S		5.06		^{2}H	0.00152 – 92.1	34
2	2.43	S		6.00		^{2}H	0.00152 – 92.1	34
3	2.35	S		7.00		^{2}H	0.00152 – 92.1	34
4	2.38	S		8.03		^{2}H	0.00152 – 92.1	34
5	2.28	S		9.18		^{2}H	0.00152 – 92.1	34
6	2.22	S		9.97		^{2}H	0.00152 – 92.1	34
7	1.02	G	110	5.95	5 mM NaPi	^{2}H	0.00152 – 5.37	40
8	1.63	G	62.1	5.66	5 mM NaPi	^{2}H	0.00152 – 5.37	40
9	1.67	G	31.1	5.73	5 mM NaPi	^{2}H	0.00152 – 5.37	40
10	5.14	G	30.5	5.79	5 mM NaPi	^{2}H	0.00152 – 5.37	40
11	1.35	G	30.5	6.03	5 mM NaPi	^{2}H	0.00152 – 5.37	40
12	2.65	G	30.4	5.90	5 mM NaPi	^{2}H	0.00152 – 5.37	40
13	1.62	G	30.3	6.41	50 mM NaPi	^{2}H	0.00152 – 5.37	40
14	1.61	G	30.5	6.23	5 mM NaPi	^{2}H	0.00152 – 5.37	40
15	1.61	G	30.4	6.39	50 mM NaPi	^{2}H	0.00152 – 5.37	40
16	1.60	G	30.6	6.70	50 mM NaPi	^{2}H	0.00152 – 5.37	40
17	1.60	G	30.6	6.92	50 mM NaPi	^{2}H	0.00152 – 5.37	40
18	1.60	G	30.6	6.87	50 mM NaPi	^{2}H	0.00152 – 5.37	40
19	1.61	G	30.4	6.09	50 mM NaPi	^{2}H	0.00152 – 5.37	40
20	1.61	G	30.4	6.75	50 mM MES	^{2}H	0.00152 – 92.1	45
21	1.61	G	30.4	6.13	50 mM NaPi	^{2}H	0.00152 – 5.37	40
22	1.65	G	29.7	6.12	50 mM MES	^{2}H	0.00152 – 5.37	40
23	1.64	G	29.9	5.99	50 mM MES	^{2}H	0.00152 – 5.37	40
24	1.65	G	29.8	6.35	50 mM MES	^{2}H	0.00152 – 5.37	40
25[e]	1.65	G	29.8	6.64	50 mM MES	^{2}H	0.00152 – 5.37	40
26	1.61	G	30.4	6.75	50 mM MES	^{2}H	0.00152 – 92.1	45
27	1.62	G	29.9	6.98	50 mM PIPES	^{2}H	0.00152 – 5.37	40
28[e]	1.62	G	29.9	6.95	50 mM PIPES	^{2}H	0.00152 – 5.37	40
29	1.62	G	29.9	7.00	50 mM PIPES	^{2}H	0.00152 – 92.1	45
30	1.62	G	29.9	7.15	50 mM PIPES	^{2}H	0.00152 – 92.1	46
31[f]	1.62	G	29.9	7.17	50 mM PIPES	^{2}H	0.00152 – 92.1	46
32	2.57	S		7.03		^{17}O	1.21 – 81.3	12
33	1.62	G	29.9	7.02	50 mM PIPES	^{17}O	0.692 – 81.3	14

[a] MbCO concentration in mM. [b] Solution (S) or gel (G).
[c] NaPi = sodium phosphate. [d] Number of data points.
[e] Measured at 5, 15, and 25 °C. [f] In presence of 8 bar Xe.

Table S2. pK_a^* Values for Titrating His Residues in Horse Mb.[a]

residue	pK_a^*		
	299.5 K, 0.2 M NaCl[1]	298 K, 20 mM NaCl[2]	298 K, 0.2 M NaCl[2]
36	7.75 ± 0.05	7.67 ± 0.01	7.80 ± 0.02
48	5.50 ± 0.07	5.42 ± 0.02	5.62 ± 0.01
81	6.86 ± 0.05	6.65 ± 0.01	6.94 ± 0.01
113	5.76 ± 0.07	5.51 ± 0.02	5.87 ± 0.02
116	6.72 ± 0.05	6.66 ± 0.02	6.79 ± 0.01
119	6.51 ± 0.05	6.38 ± 0.02	6.56 ± 0.01

[a] The number of labile His deuterons was calculated as $N_{\mathrm{LD}} = 2\sum_i [1 + 10^{\mathrm{pH}^* - \mathrm{p}K^*_{\mathrm{a},i}}]^{-1}$, where pH^* and $\mathrm{p}K^*_{\mathrm{a},i}$ are both measured in D_2O and neither are corrected for the H/D isotope effect (which largely cancels out in the difference). The set of six $\mathrm{p}K_a^*$ values used for the calculation in Sec. S1 were measured[2] at 298 K in 20 mM NaCl. In addition, we used $\mathrm{p}K_a^* = 5.91$ for His-97, determined for sperm whale MbCO.[3] The remaining four His residues are all in the basic from in the neutral pD range of interest here.[3,4]

S1. Histidine Labile-Deuteron Exchange Kinetics

We estimate the mean survival time, τ_{LD}, of the acidic imidazolium deuterons from

$$\tau_{\mathrm{LD}} = \frac{1}{k_{\mathrm{w}}[\mathrm{D_2O}] + k_{\mathrm{b}}[\mathrm{OD^-}] + k_{\mathrm{c}}\left[\mathrm{Buf^-}\right]} \ , \tag{S1}$$

where the three rate constants refer to the water, hydroxide, and buffer catalyzed exchange processes:

$$\begin{aligned} \geqslant\mathrm{ND^+} + \mathrm{D_2O} \quad &\xrightarrow{k_{\mathrm{w}}} \quad \geqslant\mathrm{N{:}} + \mathrm{D_3O^+} \\ \geqslant\mathrm{ND^+} + \mathrm{OD^-} \quad &\xrightarrow{k_{\mathrm{b}}} \quad \geqslant\mathrm{N{:}} + \mathrm{D_2O} \\ \geqslant\mathrm{ND^+} + \mathrm{Buf^-} \quad &\xrightarrow{k_{\mathrm{c}}} \quad \geqslant\mathrm{N{:}} + \mathrm{BufD} \ . \end{aligned}$$

Assuming that association and dissociation are diffusion-controlled with the rate constant k_{D}, the three LD exchange rate constants can be expressed as[5]

$$k = \frac{k_{\mathrm{D}}}{1 + 10^{\mathrm{p}K_{\mathrm{a}}(\mathrm{His}) - \mathrm{p}K_{\mathrm{a}}(\mathrm{BD})}} \ , \tag{S2}$$

where $\mathrm{p}K_{\mathrm{a}}$(His) and $\mathrm{p}K_{\mathrm{a}}$(BD) are the $\mathrm{p}K_{\mathrm{a}}$ of the acidic form of the His side-chain and of the conjugate acid BD of the base that accepts the deuteron from His, that is $\mathrm{D_3O^+}$, $\mathrm{D_2O}$, or BufD, respectively. For the following estimates, we ignore the H/D isotope effect, which largely cancels out in the $\mathrm{p}K_{\mathrm{a}}$ difference in Eq. (S2).

Taking $k_{\mathrm{D}} = 10^{10}$ $\mathrm{M^{-1}\ s^{-1}}$ (probably an overestimate), $\mathrm{p}K_{\mathrm{a}}(\mathrm{His}) = 6.38$ (the average of the values in the second $\mathrm{p}K_{\mathrm{a}}^*$ column in Table S2), $\mathrm{p}K_{\mathrm{a}}(\mathrm{H_3O^+}) = -1.74$, and $[\mathrm{D_2O}] = 55$ M, we obtain $k'_{\mathrm{w}} = k_{\mathrm{w}}[\mathrm{D_2O}] = 4.2 \times 10^3\ \mathrm{s^{-1}} \approx (240\ \mu\mathrm{s})^{-1}$. This estimate is close to the value, $k'_{\mathrm{w}} = 2.4 \times 10^3\ \mathrm{s^{-1}}$, measured by NMR for imidazole in $\mathrm{H_2O}$ at 25 °C.[6] For the hydroxide-catalyzed process, with $\mathrm{p}K_{\mathrm{a}}(\mathrm{H_2O}) = 15.74$, we obtain the estimate $k_{\mathrm{b}} = k_{\mathrm{D}} = 10^{10}\ \mathrm{M^{-1}\ s^{-1}}$. With $\mathrm{p}K_{\mathrm{a}}(\mathrm{D_2O}) = 14.95$ at 25 °C, we then obtain, at pD 7.0, $k_{\mathrm{b}}[\mathrm{OD^-}] = 10^{10} \times 10^{7.0-14.95}\ \mathrm{s^{-1}} \approx 1.1 \times 10^2\ \mathrm{s^{-1}} = (9\ \mathrm{ms})^{-1}$.

To make a significant contribution to the dominant component of the ^{2}H MRD profile (Fig. 2a), with a correlation time of ~ 5 μs, the mean survival time τ_{LD} of the labile His deuterons must also be ~ 5 μs. Our rough but conservative estimates show that the water and hydroxide catalyzed processes are too slow to contribute significantly. The buffer catalyzed

process can also be ruled out, since a tenfold increase of the phosphate buffer concentration (from 5 to 50 mM) has no significant effect on $R_1(0)$ (Fig. 2b). Furthermore, at 50 mM buffer, no variation in $R_1(0)$ was observed between the phosphate ($pK_a = 7.20$), PIPES ($pK_a = 6.76$), and MES ($pK_a = 6.15$) buffers.

A remaining possibility is an internal catalysis such as $\geqslant ND^+ \cdots O_w D \cdots {}^-OOC$, where a water molecule connects the acidic His side-chain with a nearby proton acceptor, such as a carboxylate group or a basic His side-chain. The crystal structure[7] 1DWR of equine MbCO suggests several such possibilities (Fig. S1). For example, His-36 has an upshifted pK_a (Table S2),[1,2] presumably due to the proximity of Glu-38, the carboxylate group of which is bridged to His-36 via a H-bonding water molecule (Fig. S1a).

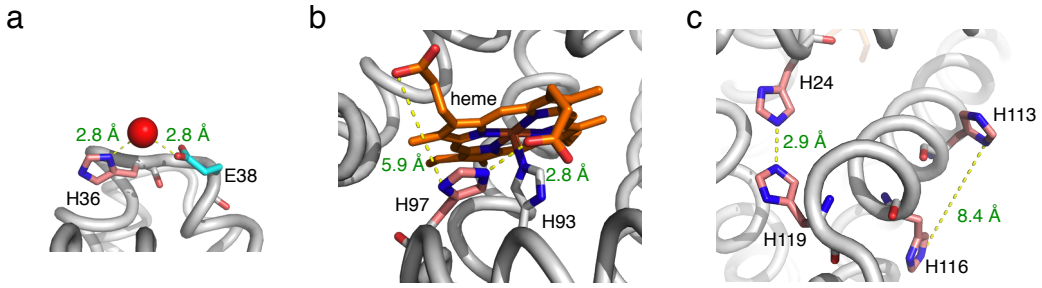

Figure S1. Possible internal catalysis of labile-deuteron exchange for (**a**) His-36, (**b**) His-97, and (**c**) His-24/His-119 and His-113/His-116. A red sphere represents a crystallographically identified water molecule.[7]

S2. pD-Dependent Effective Correlation Time

The overall correlation time, τ_C, deduced from one-component fits to solution ^{2}H MRD profiles (Fig. 3), decreases with pD even though τ_C^{eff} for the LDs increases with pD according to Eq. (3). This happens because LDs make a larger relative contribution to the MRD profile at higher pD. To understand this qualitatively, consider a single class of LDs with pD-dependent mean survival time τ_S(pD). In view of Eq. (3), we then have approximately

$$\frac{\tau_C}{\tau_R} = \frac{N^W + N^{LD}/A}{N^W + N^{LD}/\sqrt{A}} \ , \tag{S3}$$

with

$$A = 1 + \omega_Q^2 S_{iso}^2 \tau_R \tau_S(\text{pD}) \ . \tag{S4}$$

This heuristic expression predicts that $\tau_C = \tau_R$ at low pD, where τ_S is so long that the LD contribution is negligible compared to the internal-water contribution. With increasing pD, τ_S is shortened by base-catalyzed LD exchange. As a result, τ_C becomes progressively shorter than τ_R, as predicted by Eq. (S3). At still higher pD, τ_C exhibits a minimum and finally, when τ_S is so short that $A = 1$, τ_C again approaches τ_R. In practice, the minimum is not observed (at least not in our pD range) because new classes of LDs with smaller exchange rate constants gradually come into play as pD is increased.

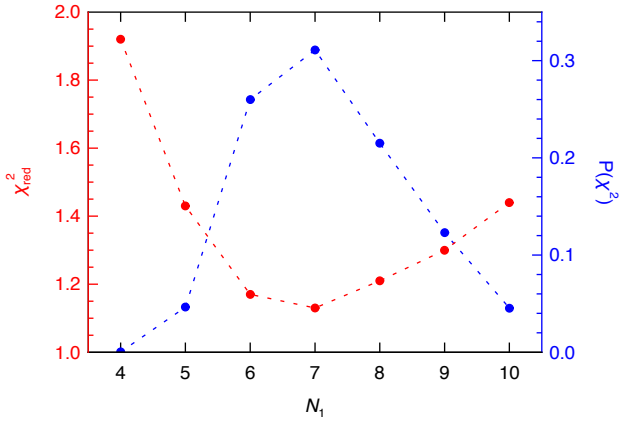

Figure S2. Reduced χ^2 and $P(\chi^2)$ for constrained fits to ^{2}H MRD profile from immobilized MbCO at pD 7.0 with N_1 for component 1 fixed in the fit.

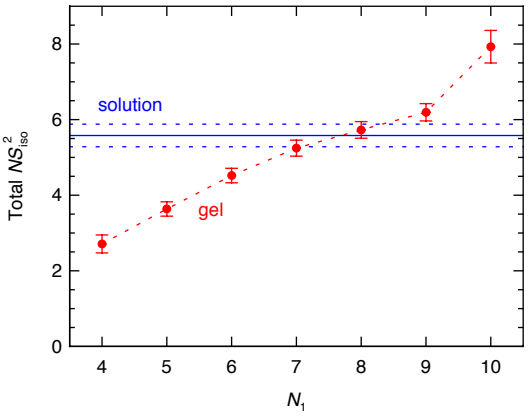

Figure S3. Amplitude parameter NS^2_{iso} from single-component fit to the solution ^{2}H MRD profile at pD 7.0 (blue line) and computed from the parameters of components 1 and 2 in constrained fits (fixed N_1) to the gel ^{2}H MRD profile at pD 7.0 (red circles).

S3. Mutual Consistency of ^{2}H and ^{17}O MRD Results

Here, we show that the parameters of the single component in the solution ^{17}O MRD profile is consistent with the results deduced from the gel ^{2}H and ^{17}O MRD profiles. To a good approximation, the product of the amplitude parameter and correlation time for the single ^{17}O solution MRD component can be expressed in terms of the parameters of the two components (identified in the gel MRD profiles) that it comprises:

$$NS_{\rm iso}^2\tau_{\rm C} = \frac{N_1^{\rm W}S_{\rm iso,1}^2\tau_{\rm R}}{1+\omega_{\rm Q}^2S_{\rm iso,1}^2\tau_{\rm R}\tau_{\rm S,1}} + N_2S_{\rm iso,2}^2\left[\frac{1}{\tau_{\rm R}}+\frac{1}{\tau_{\rm S,2}}\right]^{-1}. \qquad \text{(S5)}$$

From the fit results in Table 1, we know that $NS_{\rm iso}^2\tau_{\rm C} = 16.8 \pm 0.8$ ns and that the second term on the right-hand side of Eq. (S5) equals 8.3 ± 0.8 ns. The two components thus make comparable contributions to the solution ^{17}O MRD profile. In the first term on the right-hand side of Eq. (S5), we know that $\omega_{\rm Q} = 7.61 \times 10^6$ rad s^{-1}, $\tau_{\rm R} = 11.1$ ns, and $\tau_{\rm S,1} = 5.6$ µs (Table 1). In Eq. (S5), $S_{\rm iso,1}$ refers to the ^{17}O order parameter, which may differ somewhat from the ^{2}H order parameter, $S_{\rm iso,1} = S_1(1+\eta_1^2/3)^{1/2} = 0.80 \pm 0.02$ (Table 1). The ^{2}H order parameter pertains to internal water molecules as well as to rapidly exchanging LDs in a few His residues (Sec. 3.2).

From our analysis of the pD dependence of the gel ^{2}H MRD profiles, we estimated that component 1 comprises $N_1^{\rm W} = 5.2 \pm 0.6$ internal water molecules (Sec. 3.2). This result might be affected by modest systematic errors due to the strong covariance of N_1 and $\tau_{\rm S,1}$ in the gel ^{2}H MRD fit and to inaccuracies in our analysis of the His LD contribution (Sec. 3.2). If our analysis of the gel ^{2}H and ^{17}O MRD profiles is quantitatively consistent, Eq. (S5) should be satisfied with $N_1^{\rm W} = 5.2$ and a reasonable ^{17}O order parameter $S_{\rm iso,1}$. Figure S4 shows that Eq. (S5) is satisfied for ^{17}O $S_{\rm iso,1}$ values from below 0.5 up to 0.83 when the propagated measurement errors are taken into account. Nonetheless, over most of this $S_{\rm iso,1}$ range, Eq. (S5) predicts a smaller $N_1^{\rm W}$ value than the one deduced from the pD dependence of the gel ^{2}H MRD profiles. The ^{17}O order parameter is not likely to be substantially smaller than the ^{2}H order parameter. Assuming that $S_{\rm iso,1} = 0.80$ also for ^{17}O, we obtain $N_1^{\rm W} = 3.9 \pm 0.6$ from Eq. (S5) (Fig. S4). Taking all available MRD data into account by averaging these two $N_1^{\rm W}$ values, we arrive at the more conservative estimate $N_1^{\rm W} = 4.5 \pm 1.0$.

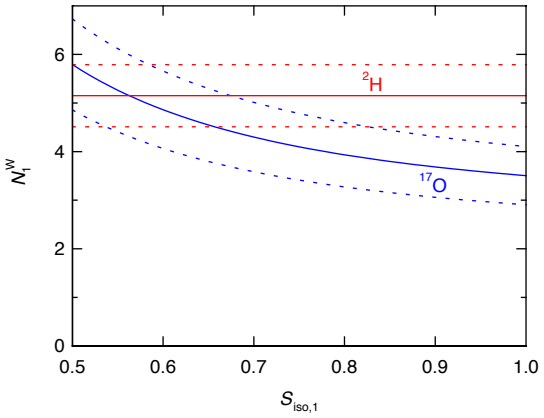

Figure S4. The number N_1^{W} of internal water molecules with MST 5.6 μs, deduced with the aid of Eq. (S5) from the solution and gel ^{17}O MRD profiles, as a function of the ^{17}O order parameter $S_{\mathrm{iso},1}$ (blue curve). Also shown is the N_1^{W} value obtained from the pD-dependent gel ^{2}H MRD profile (red line). The dotted curves or lines indicate the propagated measurement error.

S4. Determination of Xenon Occupancies

The Xe binding constants for equine Mb in the ferrous state at pH 7.0 and 25 °C have been reported as $K_1 = 94$ M^{-1} for the Xe1 site and $K_2 = 2.6$ M^{-1} for the weaker sites Xe2 – Xe4 (treated as one site).[8] We compute the Xe occupancy as

$$\theta_n = \frac{K_n[\mathrm{Xe}]}{1 + K_n[\mathrm{Xe}]} \ , \tag{S6}$$

where $n = 1$ or 2 and [Xe] is the free Xe concentration. We used ^{129}Xe NMR to determine the total Xe concentration $C_{\mathrm{Xe}} = [\mathrm{Xe}] + \theta C_{\mathrm{Mb}}$, where $\theta = \theta_1 + \theta_2$ and $C_{\mathrm{Mb}} = 1.62$ mM is the total MbCO concentration in the gel sample.

To determine C_{Xe} in the MbCO gel sample, we recorded ^{129}Xe NMR spectra (Fig. S5) from the gel equilibrated with 8 bar Xe and, for calibration purposes, from two reference samples (50 mM PIPES buffer in D_2O at pD 7.4 and cyclohexane) equilibrated with 1 atm Xe. The integrated intensity I_{Xe} of the Xe peak is proportional to the total Xe concentration C_{Xe} in the sample, but it also depends on the sample volume V (in the active region of the RF coil), the number N_{S} of accumulated scans (transients), the ^{129}Xe longitudinal relaxation rate R_1^{Xe}, and the recycle delay τ_{RD} according to

$$I_{\mathrm{Xe}} \propto C_{\mathrm{Xe}} V N_{\mathrm{S}} \big[1 - \exp\big(-R_1^{\mathrm{Xe}} \tau_{\mathrm{RD}}\big)\big] \ . \tag{S7}$$

The values of these parameters, along with the reported Xe concentration in the reference solvents (at 25 °C and 1 atm Xe) are collected in Table S3. The resulting total Xe concentrations C_{Xe} are given in Table S4, with errors propagated from the quoted intensity errors and an estimated 50 % uncertainty in R_1^{Xe} for the MbCO gel sample. The Xe occupancies θ_1 and θ_2 were then computed iteratively with the aid of Eq. (S6). In the main text, we use occupancies that are the averages of the values obtained with the two reference samples.

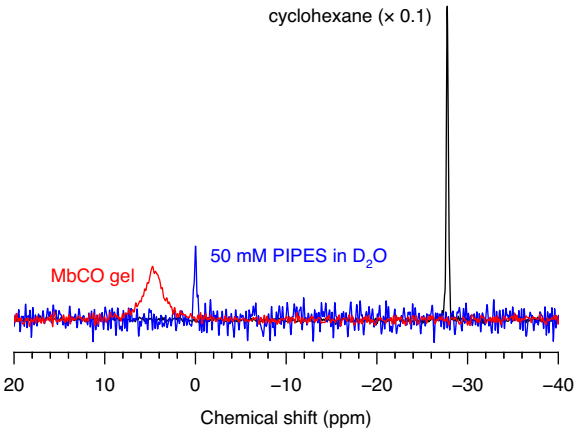

Figure S5. Natural abundance ^{129}Xe spectra recorded at 14.4 T and 25.0 °C from MbCO gel (8 bar Xe) and from the two reference samples, PIPES buffer and cyclohexane (1 atm Xe). The spectra are scaled to the same $N_S = 256$ and, in addition, the spectrum from cyclohexane was multiplied by 0.1. The ^{129}Xe chemical shift scale is referenced to the PIPES buffer sample.

Table S3. Parameters Used for Determining Xe Concentrations.

sample	I (a.u.)	C_{Xe} (mM)	V (µl)	N_S	τ_{RD} (s)	R_1^{Xe} (s^{-1})
MbCO gel	105.5 ± 1.1	–	530	2560	20.0264	0.033[a]
50 mM PIPES	1.678 ± 0.185	4.5[b]	720	256	300.0264	1.98×10^{-3} [c]
cyclohexane	33.77 ± 0.083	192[d]	710	128	60.0264	0.017[e]

[a] Estimated from ^{129}Xe spectra with different τ_{RD}. [b] Ref. 9. [c] Ref. 10. [d] Ref. 11. [e] Ref. 12.

Table S4. Xenon Concentration and Site Occupancies in MbCO Gel Sample.

reference	C_{Xe} (mM)	occupancy, θ_n	
		Xe1	Xe2 – Xe4
50 mM PIPES	34.2 ± 13.2	0.76 ± 0.07	0.08 ± 0.03
cyclohexane	51.6 ± 18.8	0.83 ± 0.05	0.12 ± 0.04
average		0.80 ± 0.09	0.10 ± 0.05

Table S5. Results of Fits to ^{2}H MRD Profiles from Immobilized MbCO at pD 7.2 and 25 °C with and without 8 bar Xe.[a]

parameter (unit)	−Xe	+Xe
$\tau_{C,1}$ (μs)	5.6 ± 0.8	[5.6]
N_1	[6.3]	6.32 ± 0.03
S_1	0.78 ± 0.02	[0.78]
η_1	0.4 ± 0.2	[0.4]
$\tau_{C,2}$ (ns)	127 ± 17	[127]
$N_2 S^2_{iso,2}$	0.69 ± 0.05	0.71 ± 0.2
$\tau_{C,3}$ (ns)	6.5 ± 1.3	[6.5]
$N_3 S^2_{iso,3}$	3.8 ± 0.8	3.6 ± 0.3
ξ_H	8.1 ± 0.8	8.3 ± 0.6
χ^2_{red}	3.15	2.38

[a] Due to slightly larger data scatter, a constrained fit was performed to the MRD profile in the absence of Xe, with $N_1 = 6.3$ fixed at the value expected from the pD 7.0 fit (Fig. 2a) and His pK_a values (Table S2). For the MRD profile in the presence of Xe, the unconstrained parameter values do not differ significantly from those obtained in the absence of Xe, demonstrating that the two data sets are indistinguishable within experimental error.

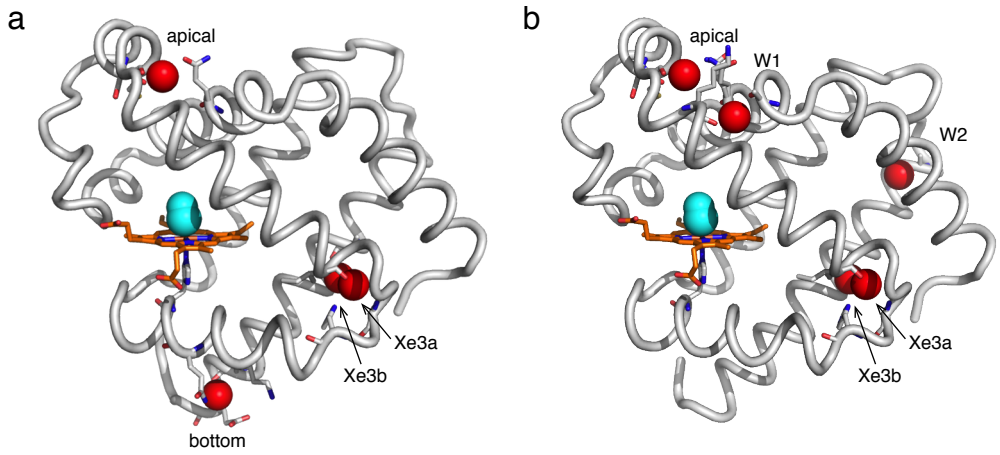

Figure S6. Internal water molecules (red spheres) in crystal structures of (**a**) equine MbCO (PDB: 1DWR[7]) and (**b**) sperm whale MbCO (PDB: 1A6G[17]) at cryogenic temperature.

Table S6. Internal Water Molecules in Crystal Structures of Horse Heart Mb.

PDB	form	res. (Å)	T (K)	pH	internal water characteristics			
					site (water no.)	occup.	B factor	H-bond acceptor/donor (length in Å)
1HRM[13]	H93Y, met?	1.70	n/a	n/a	Xe3a (160)	1.0	18.25	I75 O (2.9), G80 N (2.8), H82 $N^{\delta 1}$ (2.9), Xe3b (3.4)
					Xe3b (159)	1.0	34.00	A134 O (2.8), Xe3a (3.4)
1WLA[14]	met	1.70	n/a	n/a	DP (156)	1.0	8.26	Heme Fe, H64 $N^{\varepsilon 2}$
					Xe3a (180)	1.0	10.89	I75 O (2.9), G80 N (2.7), H82 $N^{\delta 1}$ (3.0), Xe3b (3.0)
					Xe3b (216)	1.0	38.98	A134 O (3.1), Xe3a (3.0)
					apical (217)	1.0	36.46	Q26 $N^{\varepsilon 2}$ (2.6), M55 O (2.7), S58 O (3.0)
1DWR[7]	CO	1.45	100	7.5	Xe3a (2072)	1.0	10.01	I75 O (2.9), G80 N (2.8), H82 $N^{\delta 1}$ (2.8), Xe3b (3.0)
					Xe3b (2106)	1.0	18.53	A134 O (3.0), Xe3a (3.0)
					apical (2059)	1.0	13.91	Q26 $O^{\varepsilon 2}$ (2.7), M55 O (2.8), S58 O (2.6)
					bottom (2078)	1.0	13.00	Q91 $N^{\varepsilon 2}$ (3.2), K145 O (3.0), E148 $O^{\varepsilon 2}$ (2.9)
2V1K[15]	deoxy	1.25	110	6.8	DP (2186)	1.0	32.80	Heme Fe (3.7), H64 $N^{\varepsilon 2}$ (3.6)
					Xe3a (2100)	1.0	14.13	I75 O (2.8), G80 N (2.9), H82 $N^{\delta 1}$ (2.8), Xe3b (3.0)
					Xe3b (2155)	1.0	20.92	A134 O (3.0), Xe3a (3.0)
					apical (2038)	1.0	20.87	Q26 $N^{\varepsilon 2}$ (2.6), M55 O (2.8), S58 O (2.7)
					bottom (2172)	1.0	16.89	Q91 $N^{\varepsilon 2}$ (2.9), K145 O (3.0), E148 $O^{\varepsilon 1}$ (2.6)

Table S7. Internal Water Molecules in Crystal Structures of Sperm Whale Mb.

PDB	form	res. (Å)	T (K)	pH	internal water characteristics			
					site (water no.)	occup.	B factor	H-bond acceptor/donor (length in Å)
1BZR[16]	CO	1.15	287	5.9	Xe3a (340)	1.0	18.25	I75 O (2.8), G80 N (2.9), H82 $N^{\delta 1}$ (2.8), Xe3b (3.1)
					Xe3b (403)	1.0	31.34	A134 O (3.1), Xe3a (3.1)
					apical (304)	0.65	18.07	Q26 $N^{\varepsilon 2}$ (2.9), M55 O (2.7), S58 O (2.7)
					W1 (382)	1.0	26.32	A22 O (2.7), K62 O (2.6)
1A6G[17]	CO	1.15	100	6.0	Xe3a (1006)	0.86	11.34	I75 O (2.8), G80 N (2.9), H82 $N^{\delta 1}$ (2.8), Xe3b (3.0)
					Xe3b (1056)	0.88	17.29	A134 O (2.9), Xe3a (3.0)
					apical (1053)	1.0	14.96	Q26 $N^{\varepsilon 2}$ (2.6–2.9), M55 O (2.9), S58 O (2.8)
					W1 (1011)	0.86	16.32	A22 O (2.6), K62 O (2.7)
					W2 (1154)	0.71	30.44	A127 O (2.7)
1BZ6[16]	met	1.20	287	6.0	DP (389)	1.0	8.86	Heme Fe (2.2), H64 $N^{\varepsilon 2}$ (2.7)
					Xe3a (352)	1.0	12.75	I75 O (2.8), G80 N (2.9), H82 $N^{\delta 1}$ (2.8), Xe3b (3.1)
					Xe3b (417)	1.0	34.98	A134 O (3.1), Xe3a (3.1)
					apical (509)	0.30	11.87	Q26 $O^{\varepsilon 1}$ (2.9), M55 O (2.8), S58 O (2.8)
					W1 (393)	1.0	19.83	A22 O (2.7), K62 O (2.7)
					W2 (500)	0.50	24.49	A127 O (3.0)
1A6K[17]	met	1.10	90	7.0	DP (1001)	1.0	9.70	Heme Fe (2.1), H64 $N^{\varepsilon 2}$ (2.7)
					Xe3a (1006)	0.93	10.64	I75 O (2.8), G80 N (2.8), H82 $N^{\delta 1}$ (2.7), Xe3b (3.0)
					Xe3b (1056)	0.83	14.77	A134 O (2.9), Xe3a (3.0)
					apical (1053)	1.0	11.55	Q26 $N^{\varepsilon 2}$ (2.6–3.0), M55 O (2.9), S58 O (2.8)
					W1 (1011)	0.93	13.02	A22 O (2.7), K62 O (2.7)
					W2 (1154)	0.70	23.42	A127 O (2.9)

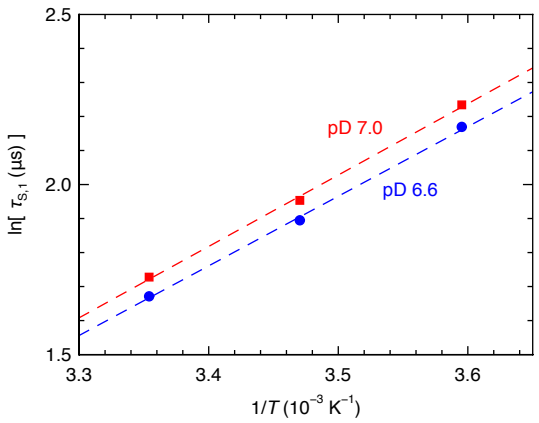

Figure S7. Arrhenius plot of the MST $\tau_{S,1}$ for component 1 in the ^{2}H MRD profile from immobilized MbCO at the indicated pD values. The slope yields $E_A = 17.4 \pm 0.4$ kJ mol^{-1} at pD 7.0 and 17.0 ± 0.3 kJ mol^{-1} at pD 6.6.

References

(1) Bhattacharya, S.; Lecomte, J. T. J. Temperature Dependence of Histidine Ionization Constants in Myoglobin. *Biophys. J.* **1997**, *73*, 3241–3256.

(2) Kao, Y.-H.; Fitch, C. A.; Bhattacharya, S.; Sarkisian, C. J.; Lecomte, J. T. J.; García-Moreno E., B. Salt Effects on Ionization Equilibria of Histidines in Myoglobin. *Biophys. J.* **2000**, *79*, 1637–1654.

(3) Müller, J. D.; McMahon, B. H.; Chien, E. Y. T.; Sligar, S. G.; Nienhaus, G. U. Connection between the Taxonomic Substates and Protonation of Histidines 64 and 97 in Carbonmonoxy Myoglobin. *Biophys. J.* **1999**, *77*, 1036–1051.

(4) Rabenstein, B.; Knapp, E.-W. Calculated pH-Dependent Population and Protonation of Carbon-Monoxy-Myoglobin Conformers. *Biophys. J.* **2001**, *80*, 1141–1150.

(5) Eigen, M. Proton Transfer, Acid-Base Catalysis, and Enzymatic Hydrolysis. Part I: Elementary Processes. *Angew. Chem. Int. Ed.* **1964**, *3*, 1–19.

(6) Ralph, E. K., III; Grunwald, E. Kinetics of Proton Exchange in the Ionization and Acid Dissociation of Imidazole in Aqueous Acid. *J. Am. Chem. Soc.* **1969**, *91*, 2422–2425.

(7) Chu, K.; Vojtchovský, J.; McMahon, B. H.; Sweet, R. M.; Berendzen, J.; Schlichting, I. Structure of a Ligand-Binding Intermediate in Wild-Type Carbonmonoxy Myoglobin. *Nature* **2000**, *403*, 921–923.

(8) Ewing, G. J.; Maestas, S. The Thermodynamics of Absorption of Xenon by Myoglobin. *J. Phys. Chem.* **1970**, *74*, 2341–2344.

(9) Wilhelm, E.; Battino, R.; Wilcock, R. J. Low-Pressure Solubility of Gases in Liquid Water. *Chem. Rev.* **1977**, *77*, 219–262.

(10) Rubin, S. M.; Spence, M. M.; Goodson, B. M.; Wemmer, D. E.; Pines, A. Evidence of Nonspecific Surface Interactions between Laser-Polarized Xenon and Myoglobin in Solution. *Proc. Natl. Acad. Sci. U.S.A.* **2000**, *97*, 9472–9475.

(11) Pollack, G. L.; Kennan, R. P.; Himm, J. F.; Carr, P. W. Solubility of Xenon in 45 Organic Solvents Including Cycloalkanes, Acids, and Alkanals: Experiment and Theory. *J. Chem. Phys.* **1989**, *90*, 6569–6579.

(12) Oikarinen, K.; Jokisaari, J. NMR Spin-Lattice Relaxation of the ^{129}Xe Nucleus of Xenon Gas Dissolved in Various Isotropic Liquids. *Appl. Magn. Reson.* **1995**, *8*, 587–595.

(13) Hildebrand, D. P.; Burk, D. L.; Maurus, R.; Ferrer, J. C.; Brayer, G. D.; Mauk, A. G. The

Proximal Ligand Variant His93Tyr of Horse Heart Myoglobin. *Biochemistry* **1995**, *34*, 1997–2005.

(14) Maurus, R.; Overall, C. M.; Bogumil, R.; Luo, Y.; Mauk, A. G.; Smith, M.; Brayer, G. D. A Myoglobin Variant with a Polar Substitution in a Conserved Hydrophobic Bluster in the Heme Binding Pocket. *Biochim. Biophys. Acta* **1997**, *1341*, 1–13.

(15) Hersleth, H.-P.; Uchida, T.; Røhr, Å. K.; Teschner, T.; Schünemann, V.; Kitagawa, T.; Trautwein, A. X.; Görbitz, C. H.; Andersson, K. K. Crystallographic and Spectroscopic Studies of Peroxide-Derived Myoglobin Compound II and Occurrence of Protonated Fe^{IV}–O. *J. Biol. Chem.* **2007**, *282*, 23372–23386.

(16) Kachalova, G. S.; Popov, A. N.; Bartunik, H. D. A Steric Mechanism for Inhibition of CO Binding to Heme Proteins. *Science* **1999**, *284*, 473–476.

(17) Vojtěchovský, J.; Chu, K.; Berendzen, J.; Sweet, R. M.; Schlichting, I. Crystal Structures of Myoglobin-Ligand Complexes at Near-Atomic Resolution. *Biophys. J.* **1999**, *77*, 2153–2174.